Asymmetric bridging of interconnected pores by encased semiflexible macromolecules

ARTICLE *in* THE JOURNAL OF CHEMICAL PHYSICS · FEBRUARY 2006

Impact Factor: 2.95 · DOI: 10.1063/1.2140704 · Source: PubMed

1 AUTHOR:

Peter Cifra
Slovak Academy of Sciences
96 PUBLICATIONS **1,025** CITATIONS

SEE PROFILE

Asymmetric bridging of interconnected pores by encased semiflexible macromolecules

P. Cifra[a)]
Polymer Institute, Slovak Academy of Sciences, Dúbravská cesta 9, 84236 Bratislava, Slovakia

(Received 3 October 2005; accepted 1 November 2005; published online 10 January 2006)

An increase of chain rigidity of macromolecule encased in interconnected cavities leads to bridging conformational transition in which polymer molecule at certain conditions spans the cavities. This is a similar phenomenon to that described for flexible chains on increase of confinement. Chain stiffness introduces, however, a delicate effect of interplay between confinement, chain stiffness, and concentration that leads to a breakup of symmetric bridging conformation to a striking asymmetric conformation even in the symmetric system of cavities. We provide the first data on this transition with complex translocation landscape and offer a tentative explanation. © *2006 American Institute of Physics*. [DOI: 10.1063/1.2140704]

I. INTRODUCTION

The translocation or threading of macromolecules through narrow pores is an important process in many biological processes as well as in a number of technologically important processes. The examples of biological processes are transport of biopolymers (proteins or DNA) through tunnels or membranes, viral injection of DNA into a host cell or biotechnology of drug delivery. Technologically important processes are such as the gel electrophoresis or membrane separation. This field, especially the aspect of biological applications, receives recently considerable attention from the perspective of experiment,[1–4] theory[5–11] as well as molecular simulations.[12–18] All these processes are primarily governed by the effect of macromolecular confinement in which the polymer coil looses the major part of its conformational entropy on translocation across the pore/channel, that represents the entropic barrier for translocation.

Since the actual systems are often complicated by biological aspects, the tests of generic issues of nonspecific physical behavior on molecular level are important. We focus here on simulation of partitioning of macromolecule between two interconnected cavities. The model of encased polymer in interconnected cavities also closely represents the situation of polymer in random porous medium. An important contribution here is the introduction of chain stiffness to translocation studies which up to now escapes most of the attention. Since many biological polymers are stiff macromolecules this is an important aspect and, as will be seen, it introduces strong effects and probably also a novel behavior.

We reported earlier results on transition to bridging conformation on increasing chain length for flexible chain encased in the interconnected cavities.[17] It was observed that longer chains, though having larger coils when free, can penetrate easier between the confining cavities when encased. This behavior is based on higher crowding in the limited space of twin cavity under the strong confinement. A question arises if similar effect also takes place if the chain length is constant in cavities but chain rigidity is increased. In this case the number of encased monomers is constant and the confining hindrance of chain arises from the increased chain rigidity in the limited space available instead.

II. METHOD

In the Monte Carlo simulation we use for the sake of efficiency and possible contact with other similar studies a coarse-grained bead-spring model in which each effective bond in chain is described by finitely extensible nonlinear elastic potential (FENE).[19] Here the bond length ℓ varies between $\ell_{\min}=2\ell_o-\ell_{\max}$ and $\ell_{\max}$, where ℓ_o is a preferred distance

$$U_{\mathrm{FENE}}(\ell) = -kR^2 \ln\left[1-\left(\frac{\ell-\ell_o}{R}\right)^2\right]. \tag{1}$$

$R=\ell_{\max}-\ell_o$ and $k/k_BT=20$ is a bond stiffness constant. Typical distances are $\ell_{\min}=0.4$, $\ell_o=0.7$ and $\ell_{\max}=1$. Most of simulations are performed for fully flexible chains; for semiflexible chains we used a bending potential[20] between two consecutive bonds

$$U_b/k_BT = b(1-\cos\theta), \tag{2}$$

where θ is a complementary angle to a valence angle and b is a bending parameter introducing the chain stiffness. For the nonbonded interactions between effective monomers we used a Morse-type potential[19]

$$U_M(r)/\varepsilon = \exp[-2\alpha(r-r_{\min})] - 2\exp[-2\alpha(r-r_{\min})] \tag{3}$$

with parameters $\varepsilon/k_BT=1$, $\alpha=24$ and a minimum of the potential at $r_{\min}=0.8$. This is a very short range potential. Interaction diminishes at $r\geqslant 1$ and the steep wall of the potential for the closest distance of segments is at $\cong 0.76$. The choice of interaction strength ε introducing the excluded volume and used in all simulations represents the good solvent condition; the theta state for flexible chain ($b=0$) is located

a)Electronic mail: cifra@savba.sk

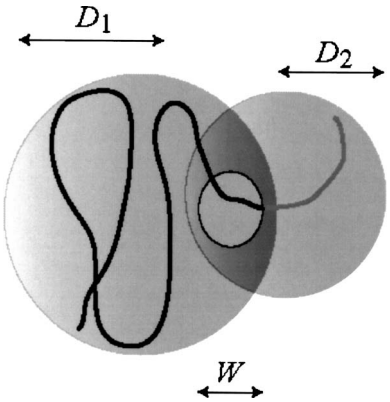

FIG. 1. Scheme of two interconnected spherical cavities with encased semiflexible macromolecule

at $\varepsilon/k_BT \approx 1/0.62$.[19] Sampling of conformations to obtain the ensemble averages within the Monte Carlo scheme was performed by reptation of chain instead of small random displacement of chain beads which is N times slower in relaxation of chain conformations.

The geometry chosen to represent the confinement by two pores in contact is formed by two interconnected spherical cavities with radii D_1, D_2 in the range of 7–20 and with a round connecting aperture of a diameter $W=4-6$, which is typically smaller than the coil and larger than the chain segment, Fig. 1. The size of aperture characterizes interpenetration of cavities and also defines the distance of two cavities. Centers of chain segments are not allowed to move out of this geometry. Since the volumes of cavities defined by the radii above restrict centers of segments, the actual wall of each cavity is at a larger radius, $D+\sigma/2$. This correction becomes important when calculating volume properties such as concentration. Volumes of two cavities are defined as partial volumes of spheres on two sides of the plane of aperture. This plane also divides the chain segments into two cavities in partitioning study. Partition coefficient, $K=\phi_1/\phi_2$, is the ratio of concentrations of chain segments in cavities 1 and 2. The extent of chain confinement is expressed relatively to the size of larger (donor) cavity D_1.

To assess the global and the local structure of encased macromolecule we estimated the form factor $S(q)$ of the polymer chain, the persistence length ℓ_{ps} in the chain and the average valence angle. The form factor was estimated according to Eq. (4)

$$S(q) = \frac{1}{N^2} \sum_{i=1}^{N} \sum_{j=1}^{N} \sin(qr_{ij})/qr_{ij}. \tag{4}$$

We used following number of effective monomers $N=100,200$ in the studied encased chain and the wave number $q=2\pi/x$ in the range from macroscopic size x to about a monomer size x; the largest q used ($q=4$) represents approximately the smallest distance x of about two bond lengths.

Persistence length ℓ_{ps} was evaluated according to the "exact" estimate as presented in Eq. (5), with a minimum number of approximations.[21] It is obtained from the average projection of an end-to-end distance of a chain onto the first bond of the chain ℓ_1. This average taken over possible configurations for the given thermodynamic state of chains is suitable for all chain models and does not depend on the state of chains, i.e., whether it is a self-avoiding chain, theta chain or ideal random chain

$$\ell_{ps} = \left\langle \sum_{i=1}^{N-1} \mathbf{l}_i \mathbf{l}_1 \right\rangle \Big/ \langle \ell \rangle. \tag{5}$$

TABLE I. Parameters for coil size and persistence length of free chains for various chain flexibility, $N=100$.

b	R_g	ℓ_{ps}/ℓ_o	$\langle R^2\rangle/\langle R_g^2\rangle$
0	4.89	1.09	6.38
1	5.3	1.30	6.32
2.5	6.3	1.92	6.34
5	8.23	3.46	6.52
10	11.0	7.95	7.06
20	13.1	13.7	8.0
35	15.9	23.1	8.99

III. RESULTS AND DISCUSSION

Parameters of free chains which are used in most of further studies on encased macromolecules in interconnected cavities are collected in Table I. The parameters include radius of gyration R_g, persistence length in unit of bond length ℓ_{ps}/ℓ_o, and a ratio of mean-square end-to-end distance and mean-square radius of gyration.

A. Penetration transition on increase of chain rigidity

We start with a long and still relatively flexible chain encased in the system of interconnected cavities, Fig. 2. The figure depicts the probability of chain conformation $P(i)$ having i segments in the cavity 1. The parameter i is considered sometimes as a translocation variable, here $i=0-200$. The barrier for translocation is also being expressed in terms of a free energy which is related to the above probability, $\Delta A(i)/k_BT=-\ln P(i)$. The parameters of the chain and cavities are $N=200$, $D=D_1=D_2=8$, $W=6$ and the chain bending energy is $b=0$, 3, 5 and 10, which leads to the confinement

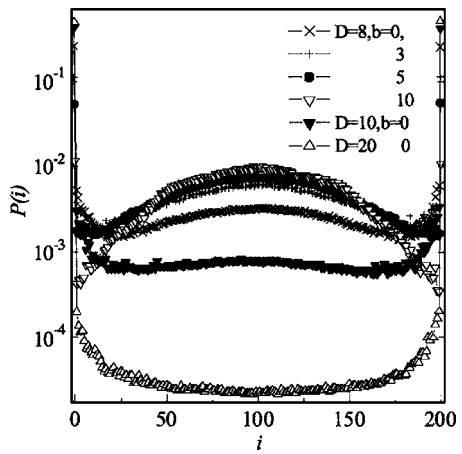

FIG. 2. Probability of chain conformation $P(i)$ having i segments in cavity 1 and $N-i$ segments in cavity 2. $N=200$ and other parameters are specified in legend.

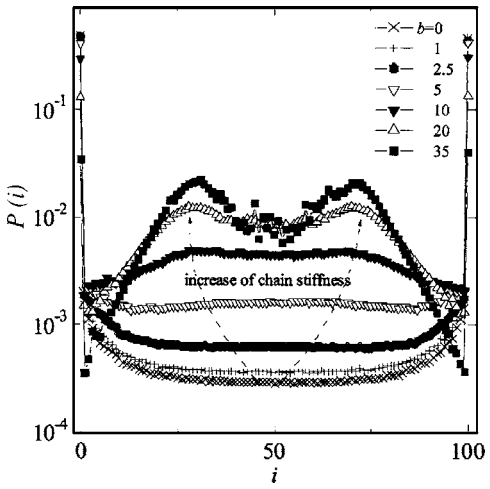

FIG. 3. Bridging transition on increasing chain stiffness and the breakup of bridging conformation into two asymmetric conformations; $N=100$, $D=10$ and chain stiffness in the range $b=0-35$ indicated in legend.

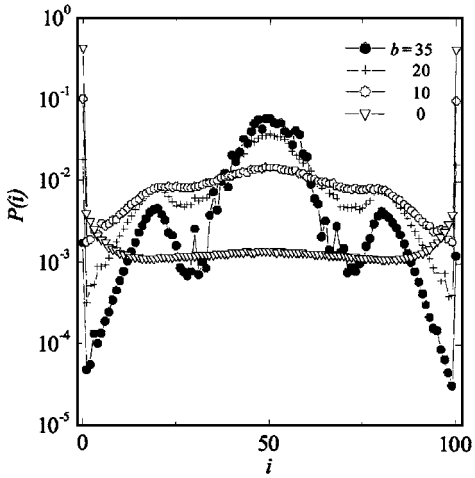

FIG. 4. Landscape of translocation probability for more confined macromolecules, $N=100$, $D=7$ and chain stiffness $b=0-35$.

for these chains in the range of $\lambda=R_g/D=0.929-2.08$. The radius of gyration of coil R_g in the confinement ratio is for free chain. For a reference flexible chains ($b=0$) in larger cavities of $D=10$ and 20 are also shown.

The figure depicts for flexible macromolecules a high probability of conformations located completely in one of the cavities with high barrier towards bridging. On increase of chain rigidity the bridging conformations start to be more populated what is visible in the increase of the probability in the middle of translocation variable. This bridging transition is expected according to the observation of similar transition on increasing concentration for flexible macromolecules. Though the concentration is not changed here, the size of coil increases with the chain rigidity at fixed geometry of cavities. As soon as the coil reaches the size of single cavity it starts to also spread to the other cavity and this is reflected in the bridge formation.

B. Change in the shape of penetration barrier on variation of chain rigidity

Stronger chain rigidities than in the previous case allow observing additional delicate effect. Results on the bridging transition for more stiff chains are shown in Fig. 3 for the system with following parameters: $N=100$, $D=10$, $W=5$ and a more extensive range of chain stiffness, $b=0-35$. The whole range of confinements is present: from simple barrier for translocation for flexible chains and moderate confinement ($b=0$, $\lambda=0.489$) up to a very stiff chain and stronger confinement ($b=35$, $\lambda=1.59$). The change in the shape of translocation probability on increasing chain stiffness features at first lowering of single barrier (or increasing probability at $i=N/2$) and than a fine effect in the form of a split of probability distribution into two relatively stable asymmetric bridging conformations.

The decrease of probability $P(i)$ when the first chain segment enters the second cavity is very steep in agreement with the theoretical prediction.[5,7,10] On entry of the first chain segment into the hole between cavities a large part of chain entropy is lost. For flexible macromolecules a broad minimum in $P(i)$ follows for partially translocated chains, $i>1$. For stiffer chains ($b=20$ and 35) with larger coils and more confined in the given cavity there is also a steep decrease of $P(i)$ at $i=1$ or $i=N$. After this, however, the probability is increasing. Once the penalty to cross the opening is paid, the further translocation is more favorable. The short penetrating subchain can increase its entropy in a larger free space of the acceptor cavity and the longer subchain which is shortening in the donor cavity has also more conformational freedom. On further penetration the probability $P(i)$ increases into a local maximum where about L' of segments is in one cavity and l' in other cavity (and vice versa for the second local maximum). The symmetric bridging conformation ($i=N/2$) is slightly less preferred than the two asymmetric conformations. A comparison of confinements and chain rigidities in Figs. 2 and 3 reveals that the split into two local maxima is governed more by increasing chain stiffness than by the confinement itself.

It should be mentioned that the partitioning of segments between two equal cavities here is given by partition coefficient $K=1$ (as in the previous case, Fig. 2) for all histograms, including also $b=20$ a 35. What does the observed structured distribution show us now?. It provides the free energy penalty during the translocation process and a distribution of possible conformations which contribute to the overall equilibrium. The bridging on increase of chain stiffness is expected according to similar bridging on increase of chain length for flexible chains.[17] However, more complex behavior is observed here in the form of asymmetric bridging for higher rigidities. This was not observed for flexible chains where symmetric bridging was observed on the increase of chain length or segment concentration.

Further increase of confinement for these rigid chains enables us to observe the coexistence of symmetric and asymmetric bridging of the cavities. In accord with this we observe for the systems characterized by parameters $N=100$, $D=7$, $W=4$, $b=0,10,20,35$ ($\lambda=0.699-2.27$) three peaks in the landscape of translocation probability, Fig. 4. A strong confinement also generates a symmetric bridge, a third local maximum in the middle of translocation variable i

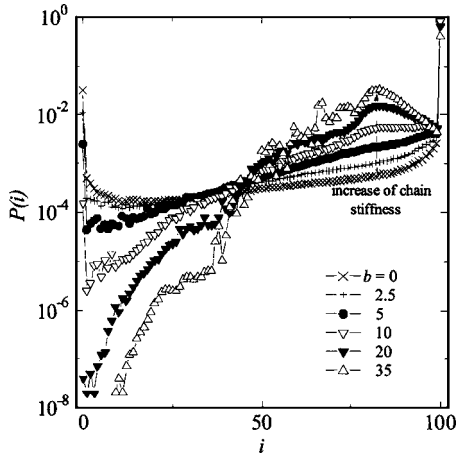

FIG. 5. Distribution of conformations in asymmetric cavities for $N=100$, $D_1=10$, $D_2=7$ and $b=0-35$.

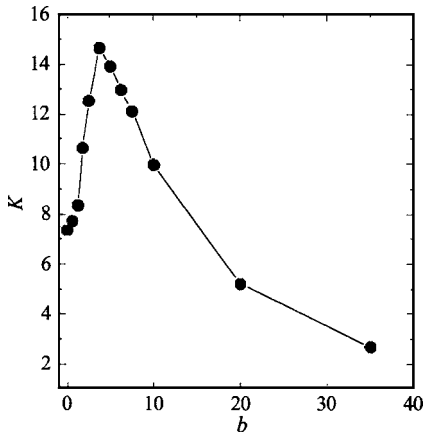

FIG. 6. Partition coefficient K in asymmetric cavities as in Fig. 5 on increase of chain stiffness.

except maintaining the two local maxima corresponding to the asymmetric bridging. Symmetric bridging conformation will prevail for even stronger confinement. Our focus will be here on the systems with two local maxima. The system with three local maxima marks the transition to symmetric bridging with a coexistence of symmetric and asymmetric bridging. Thus the system with three local maxima does not represent a more complex behavior but a range of transition instead, where the systems with symmetric and asymmetric bridging coexist for a certain range of chain rigidity and confinement. Notice that two satellite peaks move to more asymmetric positions relative to the less confined system shown in Fig. 3. We will discuss this together with the coil sizes of subchains in cavities.

What is the mechanism of formation of asymmetric bridge? We will try to answer this question after we gather more information on asymmetric partitioning, $K\neq 1$, and on properties of translocating chains.

C. Asymmetric cavities

The geometry with asymmetric cavities also reveals certain differences in comparison to the system with encased flexible chains reported earlier[17] as observed above for symmetric cavities. Figure 5 shows histograms of translocation probabilities for the system described by following parameters: $N=100$, $D_1=10$, a $D_2=7$, $W=5$, $b=0$, 2.5, 5, 10, 20 and 35. For flexible chain an asymmetric barrier due to the difference $D_1\neq D_2$ is observed in accord with previous studies of flexible chains.[5,7,10,17] On increase of rigidity we observe a change of curvature from convex to concave in the main middle range of translocation variable. For stronger rigidity we observe a clear preference of conformation with about 80% of segments in the larger cavity and the rest of the segments located in the smaller cavity. In comparison, similar distributions for flexible chains in our previous study[17] were smooth and such strong preference with a maximum as seen here was not observed. On increasing confinement of flexible chains we have seen the development of concave curvature in the middle of translocation variable, superimposed on a linear dependence between the two different decreases of probability at $i=0$ and $i=N$, but not a maximum as seen here.

Translocation landscape shown in Fig. 5 can be transformed into an average partition coefficient $K=\phi_1/\phi_2$ given by a ratio of average concentration of chain segments in the two cavities

$$K=\frac{\bar{n}_1}{N-\bar{n}_1}\frac{V_2}{V_1},\quad \bar{n}_1=\sum_{i=1}^{i=N} iP(i). \tag{6}$$

In the next figure, Fig. 6, the partition coefficient is shown as a function of chain rigidity for the states shown in the previous figure, Fig. 5. As mentioned already all results shown in the previous results, Figs. 2–4, correspond to $K=1$. In Fig. 6, concerning the system of asymmetric cavities, we observe a sharp maximum of partition coefficient for certain chain rigidity located approximately at $b=5$. An initial growth of K with rigidity b marks an increasing preference of single cavity occupancy of chain in a larger (donor) cavity. This initial growth is nonlinear and has a character of transition. It is related to the properties of semiflexible chains. An increase of coil size on increasing chain stiffness was shown to exhibit a transition on increasing chain stiffness.[21] About at $b=5$ the coil starts to fill the larger cavity, the confinement here reaches $\lambda=0.823$. For stiffer chain the segments of chain start to also penetrate the smaller cavity and the effect of segment concentration starts to prevail over the effect of chain confinement in cavities. On further increase of chain stiffness the concentration in both cavities starts to equalize and K approaches unity. A similar sharp maximum was also observed for flexible chains and similar geometry on increasing chain length.[17] In both cases the penetration to smaller cavity started when the coil size reached the size of larger cavity; either it was by an increasing chain length for flexible chains (also increasing thus the segment concentration in cavities) or by increasing the chain rigidity here while keeping constant the overall concentration in cavities.

Analysis of the effect of chain rigidity on the translocation equilibrium for macromolecule in interconnected cavities is complicated by the fact that it can rely only on ap-

proaches designed for flexible chains up to now. The free energy landscape for translocation can roughly be approximated for flexible chains in the most simple form by following terms:

$$F(i)/kT \cong (1-\gamma)\ln[i(N-i)] + iD_1^{-1/v} + (N-i)D_2^{-1/v} + \Delta\mu_1(i,\phi_1) + \Delta\mu_2(N-i,\phi_2), \quad (7)$$

where $\gamma=0.5$, $\cong 0.6$ and 1 for Gaussian ($v=0.5$), self-avoiding ($v\cong 0.6$) and rodlike chain ($v=1$), respectively. The first term represents the translocation barrier for the chain threading through the hole in solid plane/membrane.[7] This penalty for threading through the membrane hole dominates for the case of weak confinement in both cavities. Next two terms represent the confinement of subchains in the cavities 1 and 2 approximated according to Daoud and de Gennes.[22] At even higher confinement the concentration in cavities builds up and osmotic pressure starts to equilize the concentration in cavities. The effect of confinement starts to play minor role for partitioning between cavities at this point. This effect is included in classical concentration dependent chemical potential of subchains in two cavities given by the last two terms. In our previous results for flexible chains[17] a corresponding expression by Flory was used for $\Delta\mu$. This expression Eq. (7) for flexible chains produces qualitatively all curves in Fig. 2 in the range between the single cavity occupancy to the bridging conformation. For the flexible chains there exists a more precise theory.[10]

However, Eq. (7), designed for flexible chains, cannot explain the split of symmetric into asymmetric bridging. Actually, for the less flexible chains a fine balance of various effects takes place: (1) the chain confinement, (2) a drastic decrease of conformation entropy for more rigid chains relative to the flexible chains, (3) contribution of concentration/crowding for stronger confinements. Moreover, these effects are interconnected (the chain rigidity is affected by confinement, conformation entropy decreases together by confinement and by rigidity, concentration dependent chemical potential should be also affected by chain rigidity). The increased stiffness plays a role of chain length (or concentration) in the previous case of flexible chains (compare Fig. 6 here and Fig. 7 in Ref. 17), though the overall concentration here remains constant. This peculiarity arises from an increase of coil size by increasing chain stiffness which leads to a stronger confinement and crowding in the given cavity. Expressions for these effects are partially known only for flexible chains. This complex interplay requires a further development of theory and here we do not try to provide any simplified approach, instead we present the original data. A tentative explanation stems from investigation of chain properties and will be presented within the structural studies in next part.

D. Overall and local chain structure; towards understanding of asymmetric bridging

To learn more about properties of encased chain and to understand the asymmetric bridging shown in Fig. 3 we also investigate the overall and local chain structure in cavities.

The *overall structure* of encased chains represented in Figs. 2 and 3 is depicted in Fig. 7(a) and 7(b) in terms of a form factor $S(q)$ of chains. The behavior presented in Fig. 7(a) shows at a larger scale [the wave vector q below the break in $S(q)$] a compactness or strong three-dimensional confinement of encased coil. For comparison the characteristic scaling of $S(q)$ for the polymer globule is $\sim q^{-3}$. This compactness is also reflected in a lower persistence length ℓ_{ps} than for the equivalent free chain (notice next Fig. 8) and also in a coil shape factor $\langle R^2\rangle/\langle R_g^2\rangle$, which is less than 6. On smaller scale, at higher q, we observe with increasing chain stiffness an increasing range of coil structure corresponding to the structure of rigid rod along the chain with characteristic scaling $\sim q^{-1}$. This corresponds to increasing persistence length ℓ_{ps}. The picture of the form factor for systems with two peaks in Fig. 3 is similar and is shown in Fig. 7(b), only we observe a less compact structure because of weaker confinement and a more extensive range of rodlike behavior ($\sim q^{-1}$) due to higher chain stiffness.

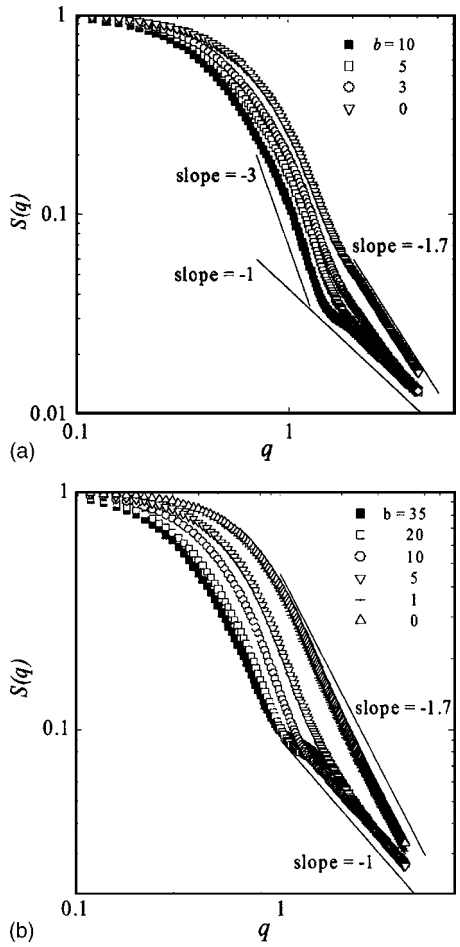

FIG. 7. Log-log plots of structure factor $S(q)$ *vs* wave number q of encased chains; (a) $D=8$, $N=200$, $b=0,3,5,10$ (Fig. 2); (b) $D=10$, $N=100$, $b=0,1,5,10,20,35$ (Fig. 3). Inserted lines next to the curves represent the slope of theoretical scaling exponents in Kratky regime for the respective state.

For further answers we now turn to the *local structure* of encased chains. Figure 8 compares encased chains represented in Fig. 2 with the free chains for the same chain stiffness. While the average bond angle along the chain backbone is the same for confined and for free chain of the same

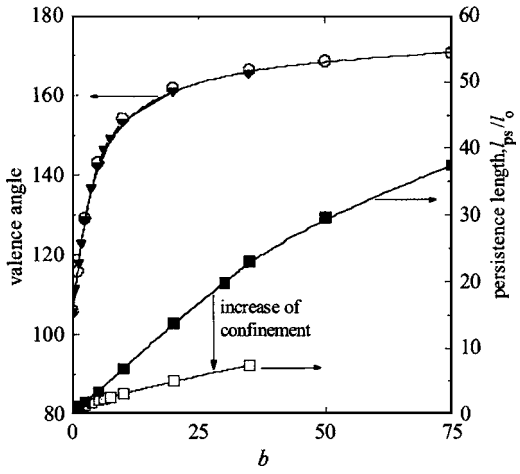

FIG. 8. Comparison of persistence length and valence angle for encased and for free chain as a function of chain stiffness. The confinement and other parameters are the same as in Fig. 3.

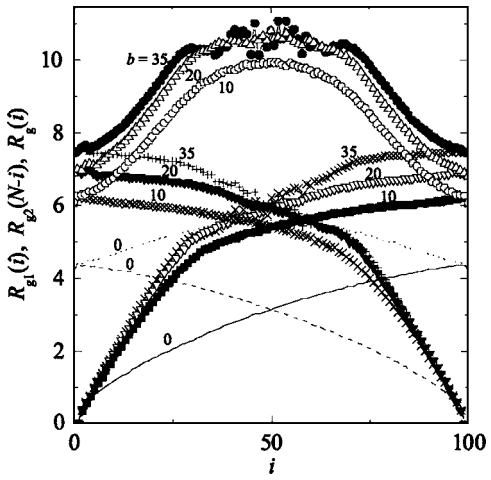

FIG. 9. Radius of gyration of subchains in cavities and of total encased chain for the states in Fig 3; $N=100$, $D=10$, and $b=0-35$.

rigidity, the persistence length is affected by confinement and cannot fully develop to the same extent as that in the free solution.

The main implication of the differences of persistence length depending on chain confinement lies in possible *explanation of surprising asymmetric bridging* seen for symmetric cavities in Figs. 3 and 4. We should not be mislead by the decrease of persistence length ℓ_{ps} by confinement. Confined chain attains smaller ℓ_{ps} relative to the free chain; however, the confined chain is not more flexible, since the valence angle in chain remains the same. Actually, due to the confinement the persistence in chain cannot develop to the extent in free chain. The number of possible chain conformations is in fact decreased by confinement through restricted rotations along the confined chain (though the persistence length in chain decreases). In this way the number of possible conformations of partial chains in cavities 1 and 2 of the bridging chain can become equal even for asymmetric conformation. This also applies thus to the entropy of subchain, the main thermodynamic driving force in the good solvent situation here. The same number of conformations of subchains can be made up either by (1) a longer and thus strongly confined subchain in one cavity with a smaller effective number of possible rotations of chain segments or (2) by a shorter and less confined part of the same chain in the other cavity but with larger number of possible rotations of chain segments. Though the restriction of conformations by confinement also operates for flexible chains, the asymmetric conformations build up only for strong chain stiffness, where the total number of chain conformations is small and rotational restriction due to confinement becomes substantial.

In order to bring more light to possible conformations of individual subchains in each cavity 1 and 2 at both sides of the hole connecting cavities, we also investigated the average radius of gyration of these subchains, $R_{g1}(i), R_{g2}(N-i)$, in two cavities as well as that of the whole chain, $R_g(i)$, as a function of extent of chain penetration between cavities i. The observed behavior shown in Fig. 9 corresponds to the system reported in Fig. 3 with the characteristic split of symmetric bridging conformation into two asymmetric conformations. Three regions are observed. The first is the range of almost linear increase of $R_{g1}(i)$ in acceptor cavity with the number of penetrated segments, $i=0-25$. This is the range of translocation in which the coil in acceptor cavity is weakly confined. On the other hand at the same time the larger part of chain, $R_{g2}(N-i)$, is still strongly confined in the donor cavity and does not decrease its size considerably with i. A break with a change into a weaker dependence of coil size $R_{g1}(i)$ on i, reflecting a more effective confinement, is observed at the same position as the first local maximum in Fig. 3, at cca $i=25-30$ for stiff chains. The second break (change of the slope) at cca $i=70-75$ represents the same effect only the longer and shorter subchains are interchanged in the two cavities. While the confinement sets in rather gradually for flexible chains ($b=0$ and 10) as seen from the smooth curves, for more rigid chains ($b=20$ and 35) a rather abrupt change in coil size is experienced at penetrations $i=25-30$.

The two subchains of penetrating chain do not have the same size R_g at the position of local maxima of conformation probability, $i=25$ or 75. This indicates that the balance leading to the asymmetry is not formed by the equality of coil sizes of subchains in two cavities, but rather by another parameter such as the entropy of subchains as explained above.

The position of local maxima of probability, Fig. 3, and the breaks on the curves on subcoil sizes, Fig. 9, are related to the size of cavities. For larger cavities, $D=10$ (Figs. 3 and 9), the coil size was increasing without confinement until $i\cong 30$ and for smaller cavities, $D=7$ (Fig. 4), this initial increase takes place until the break at $i=20$, the location of maximum of probability (coil sizes are not shown here).

The asymmetry resulting from different components contributing to the free energy of chain reminds us of relatively stable "flowerlike" conformation during the chain penetration into an adsorptive channel.[23] The chain located partially in a channel and partially in the free solution has a crown of relatively free partial chain outside of the channel and a stem of confined adsorbed subchain in the channel. The asymmetric conformation is stabilized by the adsorption of chain segments in channel, the confinement of this subchain and an entropic stabilization by segments of the crown

outside at the entrance of the channel. Here in twin cavity the confining geometry is, however, symmetrical. The observed asymmetry appears as a result of different distribution of properties of semiflexible chain over the cavities instead of different environment at different locations at the entrance of the channel or inside the channel.

The difference in persistence length ℓ_{ps} (calculated here according to the exact formula) observed for confined chains relative to the free chain have also more general implications. Often well established but approximate expressions for ℓ_{ps} (such as those using the average bond angle) are used to obtain the persistence length of macromolecules.[21] We can conclude that this procedure is allowed only for the free unconfined polymer solution.

IV. CONCLUSIONS

Expected transition towards the bridging conformation for macromolecules encased in interconnected cavities on increasing chain stiffness is confirmed. This transition is an analogy of a similar transition for encased flexible chains on increasing chain length. A novel effect and challenge for interpretation is the surprising split of symmetric bridging conformation in the system of equal cavities for strongly stiff macromolecules into two asymmetric conformations. This is in contrast to bridging of cavities by flexible chains which bridge symmetrically. This split into asymmetric bridging conformation is a fine effect superimposed on the bridging transition and is observed only for stiff chains.

The necessary condition for the formation of asymmetric bridging is the strong chain stiffness while the system with moderate stiffness under strong confinement does not exhibit the effect. Chain confinement affects the effective persistence length in chain and at the same time retains the valence angle in the chain backbone intact.

Obviously the observed effects in two interconnected cavities will also appear in larger systems of many interconnected cavities which are characteristic for random porous medium. We believe that the system of interconnected cavities is a suitable model for generic issues in these complex systems.

ACKNOWLEDGMENT

This work was partially supported by the Science and Technology Assistance Agency under the Contract No. APVT-51-044902 and VEGA 2/3013/23.

[1] J. J. Kasianowicz, E. Brandin, D. Branton, and D. W. Deamer, Proc. Natl. Acad. Sci. U.S.A. **93**, 13770 (1996).
[2] J. O. Bustamante, J. A. Hanover, and A. Liepins, J. Membr. Biol. **146**, 239 (1995).
[3] D. Nykypanchuk, H. H. Strey, and D. A. Hoagland, Macromolecules **38**, 145 (2005).
[4] A. J. Storm, J. H. Chen, H. W. Zandbergen, C. Dekker, Phys. Rev. E **71**, 051903 (2005).
[5] W. Sung and P. J. Park, Phys. Rev. Lett. **77**, 783 (1996).
[6] E. A. DiMarzio and A. J. Mandell, J. Chem. Phys. **107**, 5510 (1997).
[7] M. Muthukumar, J. Chem. Phys. **111**, 10371 (1999).
[8] M. Muthukumar, Phys. Rev. Lett. **86**, 3188 (2001).
[9] M. Muthukumar, J. Chem. Phys. **118**, 5174 (2003).
[10] C. K. Kong and M. Muthukumar, J. Chem. Phys. **120**, 3460 (2004).
[11] A. Matsuyama, J. Chem. Phys. **121**, 8098 (2004).
[12] H. C. Loebl, R. Randel, S. P. Goodwin, and C. C. Matthai, Phys. Rev. E **67**, 041913-(1–5) (2003).
[13] R. Randel, H. C. Loebl, and C. C. Matthai, Macromol. Theory Simul. **13**, 387 (2004).
[14] S. Kirmizialtin, V. Ganesan, and D. E. Makarov, J. Chem. Phys. **121**, 10268 (2004).
[15] S. Tsonchev and R. D. Coalson, Chem. Phys. Lett. **327**, 238 (2000).
[16] S. S. Chern and R. D. Coalson, J. Chem. Phys. **111**, 1778 (1999).
[17] P. Cifra, Macromolecules **39**, 3984 (2005).
[18] A. F. Sousa, A. A. C. C. Pais, and P. Linse, J. Chem. Phys. **122**, 214902 (2005).
[19] R. B. Pandey, A. Milchev, and K. Binder, Macromolecules **30**, 1194 (1997).
[20] H. Fynewever and A. Yethiraj, J. Chem. Phys. **108**, 1636 (1998).
[21] P. Cifra, Polymer **45**, 5995 (2004).
[22] M. Daoud and P. G. de Gennes, J. Phys. (Paris) 38, 85 (1997).
[23] G. F. Hermsen, M. Wessling, and N. F. A. van der Vegt, Polymer **45**, 3027 (2004).